NAIC-ID(RS)T-0558-96

NATIONAL AIR INTELLIGENCE CENTER

SELECTED ARTICLES

HUMAN TRANSLATION

NAIC-ID(RS)T-0558-96 16 January 1997

MICROFICHE NR:

SELECTED ARTICLES

English pages: 21

Source: Chinese Journal of Lasers; pp. 692-696; 722-726.

Country of origin: China
Translated by: Leo Kanner Associates
F33657-88-D-2188
Requester: NAIC/TATD/Bruce Armstrong
Approved for public release: distribution unlimited.

TABLE OF CONTENTS

GRAPHICS DISCLAIMER

All figures, graphics, tables, equations, etc. merged into this translation were extracted from the best quality copy available.

MEASUREMENT OF 2D WAVEFRONT TILT USING 1D ARRAY DETECTORS

Jiang Zhiping, Zhong Hairong,
Lu Qisheng, and Liu Zejin

Department of Applied Physics
National University of Defense Technology
Changsha 410073

Abstract: A method that uses a one-dimensional array detector to measure the two-dimensional wavefront tilt of a beam, is proposed. A preliminary experiment is given to verify the principle.

KEY WORDS: wavefront tilt, array detector.

1. Introduction

The wavefront tilt of a beam is required to be measured in numerous applications, such as adaptive optics, beam propagation through the atmosphere, automatic collimation of beams and laser beam-based measurement of the tilt of objects, etc. Generally speaking, all these problems are two-dimensional problems, in which the measurement of two-dimensional wavefront tilt is required.

Tilt measurement can be equivalent to the measurement of the beam intensity centroid, which, in earlier times, was realized using four-quadrant detectors. With the development of array devices (such as CCD photoelectric detectors), however, the four-quadrant detectors are now replaced by array detectors.

To measure the two-dimensional light intensity centroid, a face array device is required, which consists of numerous detectors (e.g., a face array CCD contains hundreds of thousands of photosensitive elements). In such devices, data are transmitted sequentially and therefore, the frame frequency cannot be high, such as 25Hz in the CCD camera, which is insufficient for rapid measurement.

Compared with face array devices, the linear array devices involve many fewer detectors and have higher a frame frequency. Now the problem is: Is it possible to use linear array devices for measuring the two-dimensional wavefront tilt? A technique of measuring the two-dimensional wavefront tilt using an one-dimensional array detector is proposed in this paper; its feasibility was verified through a preliminary experiment.

2. Principle

A. W. Lohmann et al. pointed out[1] that by placing a specially-distributed curved aperture at the incident plane of a 2f optics system (front focal plane), two one-dimensional functions, namely the Airy function and the Laguerre polynomial can be derived at the output plane (rear focal plane). With the instructions from that paper, we were considering a problem, that is: Can we use Lohmann's technique in measuring the wavefront tilt of a beam? Fortunately, the two-dimensional wavefront tilt can be changed into one-dimensional as long as a dual straight line aperture is employed.

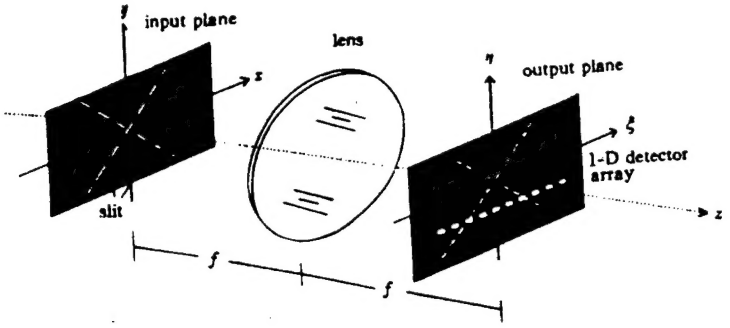

Fig. 1. Schematic diagram of the optical setup

Take the 2f optics system shown in Fig. 1 as example. Let the incident light be a plane wave that can be expressed as $\exp\left[i\frac{2\pi}{\lambda}(0_x x + 0_y y)\right]$, where 0_x and 0_y, respectively, are helical angles along x and y directions. Suppose the transmittance function of the input plane is T(x,y), then the optical amplitude of the output plane $E(\xi,\eta)$ can be calculated by using the Fourier transform as follows:

$$E(\xi,\eta) = -\frac{i}{\lambda f}\int_{-\alpha}^{\alpha}\int_{-\alpha}^{\alpha} T(x,y)\exp\left[i\frac{2\pi}{\lambda}(0_x x + 0_y y)\right]\exp\left(i\frac{2\pi}{\lambda}\frac{x\xi + y\eta}{f}\right)dxdy \tag{1}$$

where λ is wavelength; f is the focal length of lens; α is the dimension of lens. Here, for convenience, let the lens be square, which in fact is not square, and let transmittance be dual straight lines, then

$$T(x,y) = \delta(y - c_1 x) + \delta(y - c_2 x) \tag{2}$$

where the two constants c_1 and c_2, respectively, are the slope of the two straight lines. By introducing Eq. (2) in Eq. (1), the following can be derived:

$$E(\xi,\eta) = -\frac{i}{\lambda f}\int_{-\alpha}^{\alpha}\int_{-\alpha}^{\alpha}\left[\delta(y - c_1 x) + \delta(y - c_2 x)\right]\exp\left[i\frac{2\pi}{\lambda}\left(0_x x + 0_y y + \frac{x\xi + y\eta}{f}\right)\right]dxdy$$

$$= -\frac{i}{\lambda f}\left[\int_{-\alpha}^{\alpha}\exp(iC_1 x)dx \int_{-\alpha}^{\alpha}\exp(iC_2 x)dx\right] = \frac{2a}{\lambda f}\left[\mathrm{sinc}(C_1 a) + \mathrm{sinc}(C_2 a)\right] \tag{3}$$

where

$$C_i = \frac{2\pi}{\lambda}\left(0_x + 0_y c_i + \frac{\xi + \eta c_i}{f}\right), \qquad i = 1,2 \tag{4}$$

From the nature of the sinc function it is known that in Eq. (3), if $\alpha \to \infty$, then $\mathrm{sinc}(xa) \to \delta(x)$, so

$$E(\xi,\eta)\big|_{\alpha\to\infty} = \frac{2a}{\lambda f}\left[\delta(C_1) + \delta(C_2)\right] \tag{5}$$

In Eq. (5), the definition of function $\delta(x)$ is $\delta(0)=1, \delta(x\neq 0)=0$. The non-zero $E(\xi,\eta)$ in Eq. (5) should satisfy the following expression:

$$C_i = 0, \quad i = 1,2 \tag{6}$$

At the output plane, the intensity distribution is represented by two bright straight lines. From Eqs. (6) and (4), the two straight lines can satisfy the following formula:

$$\theta_x + \theta_y c_i + \frac{\xi + \eta c_i}{f} = 0, \quad i = 1,2 \tag{7}$$

(ξ_1,η_1) and $(\xi_1,\eta_1)$are, respectively, the points on the two straight lines at the output plane. By solving Eq. (7), the following can be derived:

$$\left.\begin{aligned} \theta_x &= \frac{1}{f}\,\frac{\xi_1 c_2 - \xi_2 c_1 + c_1 c_2(\eta_1 - \eta_2)}{c_1 - c_2} \\ \theta_y &= \frac{1}{f}\,\frac{\xi_2 - \xi_1 + \eta_2 c_2 - \eta_1 c_1}{c_1 - c_2} \end{aligned}\right\} \tag{8}$$

Eq. (8) implies that the two-dimensional wavefront tilt can be calculated if only the coordinates of the points on the two straight lines are measured, which can be realized with an one-dimensional array detector. For the convenience in use, Eq. (8) can be simplified. First, let a linear array detector be parallel to the ξ-axis, then η_1=η_2=constant. On the other hand, it is not difficult to understand that the measurement of wavefront tilt focuses on its variation; therefore, taking the dynamic tilt into account, Eq. (8) can be written as:

$$\left.\begin{aligned} \Delta\theta_x(t) &= \frac{1}{f}\,\frac{\Delta\xi_1(t)c_2 - \Delta\xi_2(t)c_1}{c_1 - c_2} \\ \Delta\theta_y(t) &= \frac{1}{f}\,\frac{\Delta\xi_1(t) - \Delta\xi_2(t)}{c_2 - c_1} \end{aligned}\right\} \tag{9}$$

where t is time variable; all the quantities associated with time in Eq. (9) refer to the variation relative to the time t=0. For instance, $\Delta\theta_x(t) = \theta_x(t) - \theta_x(0)$. In addition, if c_2=--c_1=1 is evaluated, then

$$\left.\begin{aligned} \Delta\theta_x(t) &= -\frac{1}{2f}[\Delta\xi_1(t) + \Delta\xi_2(t)] \\ \Delta\theta_y(t) &= \frac{1}{2f}[\Delta\xi_1(t) - \Delta\xi_2(t)] \end{aligned}\right\} \tag{10}$$

The linear array detector can also be placed parallel to axis η. In this case, the formula derived resembles Eq. (10) but essentially they are identical.

In actual measurements, α cannot be infinite, and Eq. (3) cannot be simplified as Eq. (5), yet the function sinc(x) has a main maximum at x=0. It should be understood, therefore, that the foregoing discussion is directed at the major maximum.

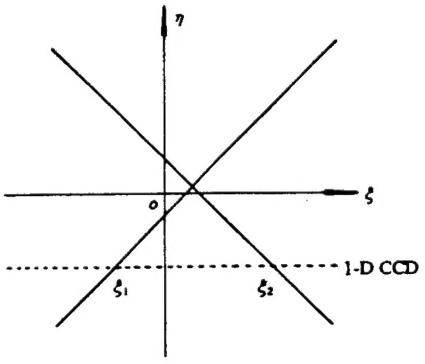

Fig. 2. Intensity distribution at the output plane

Fig. 2 is a schematic diagram showing the intensity distribution at the output plane and the location of a linear array CCD (imaginary line in the figure). Since the wavefront of the incident light is generally tilted, the two bright lines at the output plane do not cross at the original point.

3. Experimental Verification

To verify the feasibility of the foregoing concept, we conducted a simple and preliminary experiment to measure the wedge angle of an optical wedge. The experimental setup is shown in Fig. 1. The aperture in Fig. 2 was realized through photography; through photography, the two 0.3-mm-wide mutually vertical straight lines were minimized by a factor of 10, and the aperture thus

derived had a width 0.03mm (theoretically, the smaller the width of aperture, the better; however, considering its effect on the light intensity and for the convenience in making the aperture, it is appropriate to select it as approximately 0.03mm).

The laser beam emitted with an He-Ne laser device, propagating approximately 10 m, arrived at the narrow-slit aperture located at the input plane (front focal plane of the lens). The beam radius at the aperture was approximately 10mm, and the focal length of the lens was approximately 1.08m. A visible light linear array CCD was employed, with an interval of photosensitive elements 14μm, and a number of image elements 2048. The data, through an A/D converter, were processed on the computer.

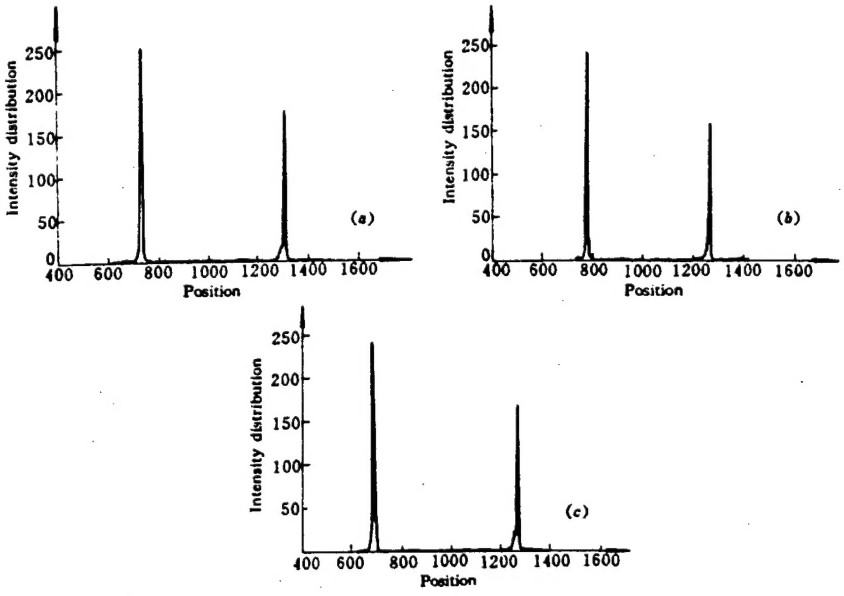

Fig. 3. CCD-detected intensity distributions
(a) original - (b) a glass plate is inserted
(c) the glass is rotated by approximately 90^0

Fig. 3 shows the intensity distribution detected with a CCD, the abscissa being the location of CCD image elements. Fig. 3(a) shows the intensity distribution without glass plates, while Fig. 3(b) shows the intensity distribution with a glass plate inserted in front of the aperture at the input plane; then, by

rotating the glass plate by 90^0, the intensity distribution was measured again [Fig. 3(c)]. In calculating the centroid of intensity distribution, the intensity distribution was properly treated with thresholds. The glass plate has a dip, just like the tilt of incident light.

Compared with Fig. 3(a), the intensity centroids of the two bright lines in Fig. 3(b) are close to each other, with much the same travel motion, and it is known from Eq. (10) that the wavefront tilt primarily goes along the y direction at this instant. The intensity centroids of the two bright lines in Fig. 3(c) simultaneously move to the left indicating that at this instant, the tilt mainly goes along the x direction [Notice: the glass plate in Fig. 3(c) has been rotated by approximately 90^0 relative to Fig. 3(b), which conforms to the measurements here]. The wavefront dips derived after data processing, respectively, are:

$$\Delta\theta_x = 0.00'$$
$$\Delta\theta_y = 1.92' \quad \text{corresponding to Fig. 3(b)} \tag{11a}$$

$$\Delta\theta_x = 1.99'$$
$$\Delta\theta_y = 0.00' \quad \text{corresponding to Fig. 3(c)} \tag{11b}$$

The dip of the glass plate is approximately 4.0', and its reflectivity is approximately 1.5; thus, the introduced dip is $\phi \approx (1.5-1)\times 4.0' = 2.0'$, basically in agreement with Eq. (11). This result shows that our measurement is reliable, and our technique is feasible. When $\phi \ll 1$, we have the expression

$$\varphi^2 = (\Delta\theta_x)^2 + (\Delta\theta_y)^2 \tag{12}$$

During the experiment, when the wavefront tilt introduced by the optical wedge was not exactly along either the x or y direction, the measurements conformed to Eq. (12). Since this was a principle-based experiment, we did not take vigorous approaches to eliminate various errors. The major error sources include: (1) The glass plate was not exactly perpendicular to the optical path,

and the wavefront tilts introduced by the glass plate in two experiments Fig. 3(b) and (c) were different, which served as the major reason for the errors in Eqs. (11a) and (11b); (2) the aperture was not placed at exactly 45^0 (i.e., $c_2=-c_1=1$ could not be strictly ensured). This is a systematic error, which can be eliminated in actual applications; (3) since the entire experimental setup was placed on an ordinary disk, the mechanical vibration system itself carries a dynamic wavefront tilt.

It is to be noted that this technique was designed to measure the wavefront tilt, but it measured even the wavefront tilt caused by mechanical vibration. With this technique to measure the two-dimensional wavefront tilt, we realized the two-dimensional stable control of beams [2]. Further studies and applications are now being underway.

4. Conclusions

This paper proposed a technique for measuring the two-dimensional wavefront tilt using linear array detectors, and verified its feasibility through an experiment. This experiment demonstrated that this technique features high-speed measurements. The frame frequency of linear array detectors are over 2 orders of magnitude higher that of face array detectors; accordingly, their measurement speed also can be more than two orders of magnitude higher (for instance, the speed can reach a few kHz), which makes these detectors available for cases, in which fast measurement is required. In principle, this technique can provide sensitivity and accuracy as high as the sensitivity and accuracy offered by linear array detectors in one-dimensional measurements as indicated in Eq. (10). The price of such detectors probably is not important, but they can be used as substitutes when only linear array devices are available.

However, this technique also suffers from some disadvantages. For instance, it may cause light intensity loss, for which it is

only applicable for high-power beams (if two mutually vertical narrow silts are replaced with two sets of mutually vertical narrow silts with numerous parallel narrow silts in either set, then the utilization rate of incident light can be increased. Such kind of aperture can be derived through photography). Although this technique cannot completely replace two-dimensional detectors, still it is useful.

The analysis and experiment presented in this paper are all preliminary. Many problems, including the effect of nonplanar wave, are expected to be solved in the future. The ideas of Lohmann et al. as well as the concepts of the authors are noteworthy. What else can we do with other apertures? The authors hope that this paper can somewhat serve as a probing attempt, which will invite more valuable papers to come.

REFERENCES

1 A. W. Lohmann, J. Ojeda-Castaneda, J. G. Ibarra. Airy function and Laguerre ploynomials: optical display processing. *Opt. Commun.*, 1994, 109 : 361~367

2. Zhong Haiyong, Jiang Zhiping, Lu Qisheng et al., "Study of beam stability based on two-dimensional wavefront tilt measurement using one-dimensional array detectors," in press.

This paper was received for editing on September 4, 1995, and the edited paper was received on November 6, 1995.

TEN-THOUSAND WATT LASER LARGE AREA AUTOMATIC SPREADING SYSTEM

Among the "Eighth Five-Year Plan" key projects, the laser machining center affiliated with Tianjing Textile College successfully developed an automatic 10,000-W watt large-area laser spreading system, which consists of a 10 kw laser-based spreading wide-band scan rotating mirror, and a laser spreading automatic powder spray machine. The scanning mirror has two functions: wide band and focusing scan, with a scanning width 10~50 nm continuously adjustable, and a scanning frequency of 60,000times/second

continuously adjustable. In the scanning band, the beam distribution is uniform. The automatic powder spray machine adopts adjustable rotating drum material level measurement, combined with non-carrier gas powder delivery, the powder delivery being continuous, uniform and stable. The powder quantity delivered is large and can reach 0.5~200g/min continuously adjustable; the precision of powder delivery is ≤2%; powder utilization rate can reach 98%. The materials to be delivered cover a wide range, including not only ordinary Ni base, Fe base and Co base, but also super-fine ceramic powder and super-heavy WC powder. The single-channel spreading width (10~35nm) and single-channel spreading thickness (0.2~8 nm) allow a wide range of adjustment.

With the foregoing rotating mirror and powder spray machine, a long-time laser spreading test was conducted on a ø500 large roller. The test shows that the above-mentioned system worked over 10 consecutive hours with 8-kw CO_2 laser spreading, and its reliability index met the requirements from the State Reliability Center.

This achievement proves to be a significant invention in aspects such as 10,000-W laser wideband rotating mirror linear spot-scan technology, powder delivery mechanism, wideband non-carrier gas powder delivery, and other measures needed for industrial production. Also, this system well conforms to conditions prevailing in China. Its overall level can keep up with the international advanced level. This accomplishment was certified by the related department of this country in January 1996 and began to be applied in laser spreading and quenching with respect to multiple rollers below ø500, automobile rocker arms, convex axles and automobile oil seal, bringing about great economic and social benefits.

LIMIT OF ANISOPLANATISM TO LASER-GUIDE-STARS

Fan Chengyu and Song Zhengfeng

Anhui Institute of Optics and
Fine Mechanics
Chinese Academy of Sciences
Hefei 230031

Abstract: The main limit for a laser-guide-star adaptive-optics-system is the focal anisoplanatism. Firstly, based on the filter function of the atmospheric turbulence sensing geometry, the variance of the residual wave-front distortion resulting from focal anisoplanatism was derived, then the effective diameter d_0 of the imaging system was derived. d_0 was calculated according to the atmospheric turbulence model in Kunming and Xinglong. The calculation shows that the correction of the piston and tilt is important for the adaptive optics system.

KEY WORDS: laser-guide-star, adaptive optics, focal anisoplanatism.

1. Introduction

Placing an adaptive optics system (AOS) in the traditional ground-based astronomical telescope proves to be an important means for upgrading imaging quality. In this case, the acquisition of a beacon source in the AOS is a key problem; the beacon is supposed to lie within the isoplanatic angle of the

target to be measured. It is well understood that in the range of visible light and infrared light, the isoplanatic angle is extremely small, generally only a few angular seconds. In this range, there is no naturally-originated guide star (NOGS) available. To solve the problem of guide stars applicable in astronomical observations, Feinleib[1] in 1982, and Foy and Labeyrie[2] in 1985, respectively, proposed the concept of using Rayleigh scattering or sodium resonant scattering as artificial guide stars (AGS) in AOS, and later made quite a few successful demonstrations.

Since the height of the AGS is limited, the spherical waves from the AGS and the plane waves from celestial bodies, while passing through atmospheric turbulence and arriving at receiving apertures along different paths, can form an anisoplanatic region, or so-called focal anisoplanatism.

This paper primarily discusses the limits of focal anisoplanatism over the AOS. First, the authors derived the formula for the effective diameter d_0 as a measure of the focal anisoplanatism. Then, based on the calculations of the atmospheric turbulence models in Kunming and Xinglong, the authors demonstrated that d_0 is closely associated with the distribution of atmospheric turbulence, and that the correction of the phase distortion of low-order terms is significant to the AOS.

2. Basic Formulas

According to the analysis made by Fried[3], for a circular aperture receiving system, a spherical wave from beacon source and a plane wave from a celestial body can generate a variance of residual wavefront distortion due to focal anisoplanatism as shown in Fig. 1, which can be expressed as:

$$E^2 = (D/d_0)^{5/3} \tag{1}$$

where D is the diameter of the aperture of a receiving telescope; d_0 is the effective diameter of the AOS.

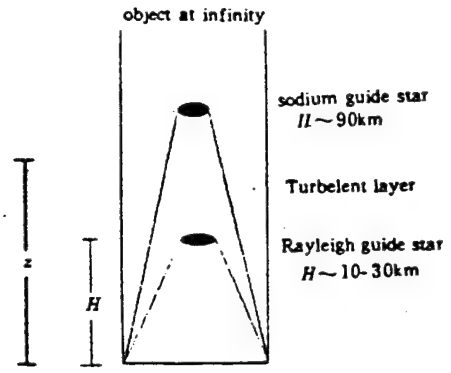

Fig. 1. Diagram of artificial guide stars

Here, the main requirement is to calculate E^2; taking advantage of the systematic integration average of the phase structure function at the plane of the receiving aperture, it will be fairly easy to derive the general expression for calculating the variance of the residual wavefront distortion resulting from the focal anisoplanatism[4] as follows:

$$E^2 = 0.207k_0^2 \int_0^\infty C_n^2(z)\left[\int f(K)g(K,z)\mathrm{d}K\right]\mathrm{d}z \tag{2}$$

where $k_0=2\pi/\lambda$, λ is beacon wavelength; the integration of z extends from the receiving aperture to the celestial body of interest; the integration of K is a two-dimensional space at the plane of the receiving aperture; f(K) is the atmospheric turbulence spectrum, which, in our case, is the normalized Kolmogorov turbulence spectrum

$$f(K) = K^{-11/3} \tag{3}$$

g(K,z) is the aperture filter function representing the sensing geometry of turbulence, which takes different forms with

reference to different problems.

First, we consider the variance of the residual wavefront distortion under the height of the beacon. In accordance with the analysis made by Sasiela[4], when the piston and tilt are retained, the filter function takes on the following form:

$$g(K,z) = 2\left\{1 - \frac{2J_1[KD(H-z)/2H]}{KD(H-z)/2H}\right\} \tag{4}$$

By introducing Eqs. (3) and (4) in Eq. (2), and integrating the azimuth angle of space K, the distortion variance in the presence of the piston and tilt can be derived as follows:

$$E_1^2 = 2.606k_0^2 \int_0^H dz C_n^2(z) \int_0^\infty dK K^{-8/3}\left\{1 - \frac{2J_1[KD(H-z)/2H]}{KD(H-z)/2H}\right\} \tag{5}$$

Finally, through simplified calculations, the distortion variance expressed with part of the turbulence moments can be obtained as follows

$$E_1^2 = 0.5007k_0^2 \sec\phi (D/H)^{5/3} \mu_{5/3}^1(H) \tag{6}$$

Here, the definition for some of the m-order turbulence moments is: for the lower part of the beacon

$$\mu_m^1 = \int_0^H dz z^m C_n^2(z) \tag{7}$$

and for the upper part of the beacon

$$\mu_m^1 = \int_H^\infty dz z^m C_n^2(z) \tag{8}$$

Normally, researchers are interested in the situation after the piston and tilt are corrected. Based on Eq. (2) and the filter functions of the piston and tilt, the distortion variance caused by the piston and tilt can be calculated separately.

Moreover, as long as the variance of the piston, or the variance of the piston and tilt is subtracted from Eq. (6), the residual variance can be calculated after the piston, or the piston and tilt are corrected.

The filter function of the piston and tilt can be written as follows[4]

$$g_z(K,z) = 4v^2\left\{\frac{J_*(KD/2)}{KD/2} - \frac{J_*[KD(H-z)/2H]}{KD(H-z)/2H}\right\}^2 \tag{9}$$

where subscript z represents piston (P) and tilt (T); it represents the piston when v=1 and represents the tilt when v=2. Through substituting Eq. (9) in Eq. (2), and integrating the azimuth angle of space K, the following can be derived:

$$E^2_{\gamma z} = 1.303k_0^2\int_0^H dzC_n^2(z)4v^2\int dKK^{-8/3}\left\{\frac{J_*(KD/2)}{KD/2} - \frac{J_*[KD(H-z)/2H]}{KD(H-z)/2H}\right\}^2 \tag{10}$$

Then, by introducing the variable x=KD/2, y=(H-z)/H, and inserting an additional term with zero as a sum, we obtain

$$E^2_{\gamma z} = 1.642k_0^2D^{5/3}\int_0^H dzC_n^2(z)I(z) \tag{11}$$

$$I(z) = \int_0^\infty dxx^{-14/3}\left\{\left[J_*^2(z) - \frac{a^2x^2}{4}\right] + \left[\frac{1}{y^2}J_*^2(xy) - \frac{a^2x^2}{4}\right] - 2\left[J_*(z)J_*(xy)/y - \frac{a^2x^2}{4}\right]\right\} \tag{12}$$

The additional term is introduced in Eq. (12) so that the integration can converge when the piston is calculated; α=1 is selected in calculating the piston, and α=0 in calculating the tilt.

According to the Mellin transformation technique developed by Sasiela[5], the variance of piston distortion can be calculated as

$$E^2_{\gamma P} = 0.0833k_0^2\sec\phi D^{5/3}\mu_2^{\frac{1}{2}}(H)/H^2 \tag{13}$$

and the variance of tilt distortion is

$$E^2_{\uparrow T} = 0.368 k_0^2 \sec\phi D^{5/3} \mu_2^{\uparrow}(H)/H^2 \tag{14}$$

By subtracting Eq. (13) from Eq. (6), the variance of residual distortion after the piston is corrected can be derived as

$$E^2_{\uparrow PR} = k_0^2 \sec\phi D^{5/3} [0.5007 \mu_{5/3}^{\uparrow}(H)/H^{5/3} - 0.0833 \mu_2^{\uparrow}(H)/H^2] \tag{15}$$

By subtracting Eqs. (13) and (14) from Eq. (6), the variance of residual distortion after the piston and tilt are corrected can be obtained as

$$E^2_{\uparrow TTR} = k_0^2 \sec\phi D^{5/3} [0.5007 \mu_{5/3}^{\uparrow}(H)/H^{5/3} - 0.4513 \mu_2^{\uparrow}(H)/H^2] \tag{16}$$

For the effects of turbulence in the upper part of the beacon, the variance of residual phase distortion can be derived by using the Zernike model proposed by Noll[6]. After the piston is corrected, the following can be obtained:

$$E^2_{\uparrow PR} = 1.0299 (D/r_0^{\uparrow})^{5/3} \tag{17}$$

Here, the atmospheric coherent length $r_0^{\uparrow}$, calculated above the beacon height, can be expressed as

$$r_0^{\uparrow} = [0.423 k_0^2 \mu_0^{\uparrow}(H)]^{-3/5} \tag{18}$$

Hence,

$$E^2_{\uparrow PR} = 0.436 k_0^2 \sec\phi D^{5/3} \mu_0^{\uparrow}(H) \tag{19}$$

Similarly, the residual variance after the piston and tilt are corrected is

$$E^2_{\uparrow TTR} = 0.134 \left(\frac{D}{r_0^{\uparrow}}\right)^{5/3} \tag{20}$$

i.e.,

$$E^2_{\uparrow TTR} = 0.057 k_0^2 \sec\phi D^{5/3} \mu_0^{\uparrow}(H) \tag{21}$$

Thus, by adding Eqs. (15) and (19), the distortion variance

caused by focal anisoplanatism after the piston and tilt are corrected is

$$E_{PR}^2 = E_{1PR}^2 + E_{\uparrow PR}^2 = k_0^2 \sec\phi D^{5/3}[0.436\mu_0^2(H) + 0.5007\mu_{5/3}^2(H)/H^{5/3} - 0.0833\mu_2^2(H)/H^2] \quad (22)$$

Similarly, by adding Eqs. (16) and (21), the variance of residual wavefront distortion after the piston and tilt are corrected is

$$E_{PTR}^2 = E_{1PTR}^2 + E_{\uparrow PTR}^2 = k_0^2 \sec\phi D^{5/3}[0.057\mu_0^2(H) + 0.5007\mu_{5/3}^2(H)/H^{5/3} - 0.4513\mu_2^2(H)/H^2] \quad (23)$$

By introducing Eqs. (22) and (23), respectively, in Eq. (1), the expressions for d_{OPR} after the piston is corrected, and d_{OPTR} after the piston and tilt are corrected can be derived as follows:

$$d_{OPR} = k_0^{-6/5}\cos^{3/5}\phi[0.436\mu_0^2(H) + 0.5007\mu_{5/3}^2(H)/H^{5/3} - 0.0833\mu_2^2(H)/H^2]^{-3/5} \quad (24)$$

$$d_{OPTR} = k_0^{-6/5}\cos^{3/5}\phi[0.057\mu_0^2(H) + 0.5007\mu_{5/3}^2(H)/H^{5/3} - 0.4513\mu_2^2(H)/H^2]^{-3/5} \quad (25)$$

The expression for d_0 that includes the piston and tilt can be derived through making a slight change in Eq. (6), i.e., by expressing part of atmospheric turbulence moments as omnidistance atmospheric turbulence moments, and then inserting them in Eq. (1) as follows:

$$d_0 = k_0^{-6/5}\cos^{3/5}\phi\left(\frac{0.5007\mu_{5/3}}{H^{5/3}}\right)^{-3/5} \quad (26)$$

3. Atmospheric Turbulence Models

In November 1992, Zeng Zhongyong et al. from the Anhui Institute of Fine Mechanics recorded measurements of the height distribution of $C_n^2(h)$ by using a balloon-borne exploring meter in Kunming and Beijing and obtained huge amounts of data. We analyzed the measurement data from Kunming and fitted them with the Hufnagel model. The Hufnagel model is as follows:

$$C_n^2(h) = a_1 h^{\alpha}\exp\left(-\frac{h}{H_1}\right) + a_2\exp\left(-\frac{h}{H_2}\right) + a_3\exp\left(-\frac{h}{H_3}\right) \quad (m^{-2/3}) \tag{27}$$

where α_1, α_2, α_3, H_1, H_2, H_3 and α are all fitted constants; h is the height above the ground, and is given in units of m. Based on the time of measurement, three models were built, namely morning, night, and average. The fitted parameters are shown in Table 1, of which the data from Xinglong were derived from reference [7]. Fig. 2 shows the Kunming-average measured data, and the model-fitted curves.

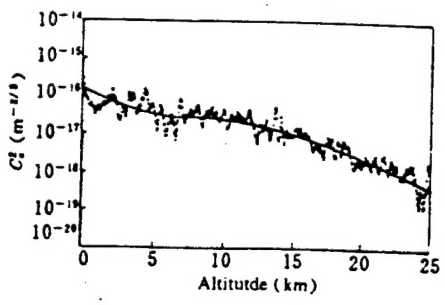

Fig. 2. $C_n^2(h)$ versus height at Kunming (in Nov. 1992)
The squares: the measured data; solid curve: the fitted data

4. Calculations

Taking advantage of the Kunming atmospheric turbulence model and HV5/7 model introduced in the previous section, we calculated d_0. The calculations were based on both Kunming and Xinglong average turbulence models; in addition, for comparison, the HV5/7 [8] model was also calculated. Fig. 3 (a), (b), and (c) show, respectively, the calculations associated with the turbulence

TABLE 1. Parameters of Vertical Distribution of $C_n^2(h)$

Site	Date	a_1	$a_2(m^{-2/3})$	$a_3(m^{-2/3})$	H_1(m)	H_2(m)	H_3(h)	α
Kunming	Average	1.0E-38	1.5E-16	0	1600	2800	∞	6
	Morning	3.07E-38	2.5E-16	0	1500	2150	∞	6
	Night	3.41E-40	5.0E-16	0	1750	5000	∞	6
Xinglong	Average	12.52E-53	9.1E-16	2.0E-15	990	1305	520	10
	Morning	19.36E-53	2.7E-16	8.0E-15	971	2200	501	10
	Night	9.68E-53	8.1E-16	3.0E-15	990	2800	812	10

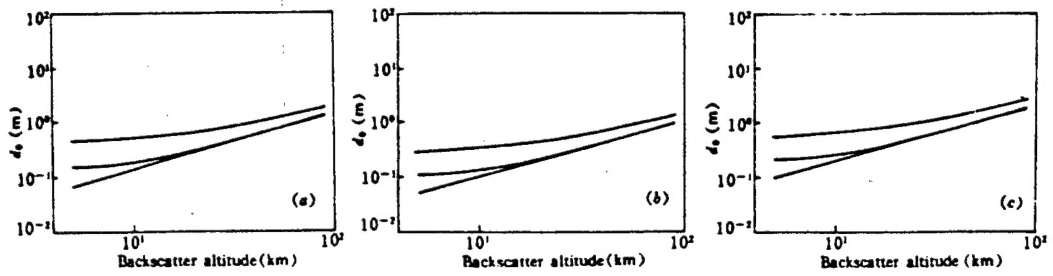

Fig. 3. Adaptive optics system effective diameter d_0 plotted as a function of laser beacon height for various turbulence models (a), (b) and (c). The results associated with the turbulence model Kunming-average, Xinglong-average, HV5/7, respectively. In each figure, the curves correspond to propagation at zenith with an operating wavelength equal to 0.5 μm. The upper curve in each figure is for the case in which the piston and the tilt are corrected. The middle is for the case in which the piston is corrected. The lower is for the case in which the piston and tilt are included.

model Kunming-average, Xinglong-average, and HV5/7. During the calculations, the zenith ψ was assumed to be equal to zero with an operating wavelength λ equal to 0.5μm. The upper curve in each figure, derived from Eq. (25), is for the case in which the piston and tilt are corrected; the middle curve, derived from Eq. (24), is for the case in which the piston is corrected, while the lower curve, derived from Eq. (26), is for the case in which the piston and tilt are included in wavefront distortion.

It can be seen from these calculations that the value of d_0 is closely related to the distribution of $C_n^2(h)$, and depends on the height of the AGS and the content of correction. Let us take the Kunming turbulence model as example; if the height of the AGS is 15km, d_0 will be less than 0.22m before correction, and increase to approximately 0.58m after the piston and tilt are corrected. This means that with an 0.6-m aperture telescope and Rayleigh scattering at the height 15km as the AGS, the variance of residual wavefront distortion can decrease from 5.3rad^2 to

$1.06rad^2$ after the piston and tilt are corrected. In other words, at this instant, the Strehl ratio of the system ($SR=\exp\{-E^2\}$ can attain 0.35 compared with the 0.0049 value of the Strehl ratio before correction. As Close and McCarthy Jr. [9] confirmed, when SR~0.14, a star image that approaches the diffraction limit can be derived, whose half-peak width is 0.19". Hence, it is possible for the foregoing system to derive a high-quality star image in Kunming.

Finally, it is to be noted that the above calculations were conducted with reference to visible light. Since d_0 is directly proportional to $\lambda^{6/5}$, the calculations are also applicable for other wavelength, if only a ratio coefficient is multiplied. Obviously, at wavelength farther than infrared wavelength, the effects of the AGS correction will be even more remarkable.

REFERENCES

1 J. Feinleib. Proposal 82-P4. Adaptive Optics Associates, Cambridge, Mass., 1982

2 R. Foy, A. Labeyrie. Feasibility of adaptive telescopy with laser probe, *Astron. Astrophys*, 1985, 152 : 129～131

3 D. L. Fired, J. F. Belsher. Analysis of fundamental limits to artifical-guide-star adaptive-optics-system performance for astronomical imaging. *J. Opt. Soc. Am.*, 1994, A11(1) : 277～287

4 R. J. Sasiela, J. D. Shelton. Transverse spectral filtering and Mellin transform techniques applied to the effect of outerscale on tilt anisoplanatism. *J. Opt. Soc. Am.*, 1993, A10(4) : 646～660

5 R. J. Sasiela, J. D. Shelton. Mellin transform techniques applied to integral evaluation: Taylor series and asymptotic approximation. *J. Math. Phys.*, 1993, 34 : 2572～2617

6 R. J. Noll. Zernike polynomials and atmospheric turbulence. *J. Opt. Soc. Am.*, 1976, 66(3) : 207～211

7. Wu Xiaoqing, Zeng Zhongyong, Ma Chengsheng et al., "Analysis of entire atmospheric turbulence in Xinglong," Quantum Electronics, 1996, to be published.

8 R. E. Hufnagel. Variation of atmospheric turbulence, in Digest of Topical Meeting on optical propagation through turbulence. Optical Society of American, Washington, D. C., 1974. WA1

9 L. M. Close, D. W. McCarthy, Jr.. High-resolution imaging with a tip-tilt Cassegrain secondary, PASP, 1994, 106 : 77～87

This paper was received for editing on August 1, 1995, and the edited paper was received on January 2, 1996.